

1 **Fe-based metallic Glass**
2 **Catalyst with Nanoporous Surface for Azo Dye degradation**

3 Z. Deng^{a,b,#}, X.H. Zhang^{c,a#}, K. C. Chan^{a*}, L. Liu^b, T. Li^b

4 a. Advanced Manufacturing Technology Research Centre, Department of Industrial
5 and Systems Engineering, The Hong Kong Polytechnic University, Hong Kong

6 b. State Key Lab for Materials Processing and Die & Mould Technology, School of
7 Materials Science and Engineering, Huazhong University of Science and
8 Technology, Wuhan 430074, China

9 c. Jiangsu Key Laboratory of Advanced Metallic Materials, School of Materials
10 Science and Engineering, Southeast University, Nanjing 211189, China,

11 # These authors contributed equally to the work

12 * Corresponding author

13 **Abstract**

14 In this work, porous structures were introduced to the surface of Fe-based metallic
15 glass ribbons for the first time by chemical treatment in order to increase the catalytic
16 activity in the degradation of azo dyes. The results show that etching treatment in an
17 HF solution with a volume concentration of 20 % for 40 min leads to a porous
18 structure on the Fe-Si-B-Nb metallic glass with a dramatic increase in the specific
19 surface area by 25 times. The much higher specific surface area of the porous ribbons
20 greatly improves the catalytic activity in the degradation of Direct Blue 15 when
21 compared with as-spun metallic ribbons.

22 **Keywords:** Nanoporous surface; Fe-based metallic glasses; Catalytic properties; Azo

1 dyes degradation.

2 **1. Introduction**

3 Nowadays, dye containing wastewater is widely generated in the dyestuff, textile,
4 paper and plastics industries (Mester and Tien 2000, Peralta-Hernández et al., 2008,
5 Wojnárovits and Takács 2008). Dye containing wastewater includes refractory
6 materials and biological toxic substances which can cause serious environmental
7 contamination. Current approaches, such as carbon sorbent absorption (Malik 2004,
8 Santhy and Selvapathy 2006), bacterial degradation (Sarataleet et al., 2011, Baeta et
9 al., 2015) and reduction reaction by zero-valent metals (Lin et al., 2008, Ma and
10 Zhang 2008, Li et al., 2015) have been used to degrade the contaminants, in which
11 reduction reaction by zero-valent metals has attracted a lot of attention due to low cost,
12 simple operation and efficient degradation capability. Among these approaches, zero-
13 valent iron has been successfully applied for wastewater treatment owing to its
14 excellent catalytic properties for dissociating various organic chemicals (Chen et al.,
15 2011, He et al., 2012, Fu et al., 2014, Segura et al., 2015). However, traditional zero-
16 valent iron easily oxidizes or forms a hydroxide on the surface during the reaction
17 process, leading to a lower catalytic activity (Xiao et al., 2015).

18 Amorphous alloys have attracted increasing attention in many fields due to their
19 unique disordered structure (Greer 1995, Wang 2009, Guo et al., 2015, Phan et al.,
20 2015). In addition, the amorphous alloy is an ideal choice for wastewater treatment
21 because of its metastable state (Schroers 2008). Recently, Fe-based amorphous alloys
22 have been reported to show high catalytic activity in the degradation of organic
23 chemicals, such as azo dyes (Wang et al., 2012, Zhang et al., 2012, Liu et al., 2014,
24 Scaglione and Battezzati 2015, Tang et al., 2015). Fe-based metallic glass has a higher

1 catalytic activity compared to corresponding crystallize materials, and is attributed to
2 the lower activation energy for electron transfer (Das et al., 2015). On the other hand,
3 Fe-based metallic glasses ribbons also show good stability in degradation processes,
4 and can be recycled at least 4 times with high degradation efficiency (Zhang et al.,
5 2012). However, few studies have been reported that discuss the factors affecting the
6 catalytic activity, such as the morphology or size of the catalyst. It was reported that
7 ball-milled Mg-based amorphous alloy powders have a much better capability in
8 degrading azo dyes due to the ball-milling causing high roughness on the surface in
9 comparison to Fe-based metallic glasses powders (Wang et al., 2012). On the other
10 hand, with the disadvantages of the recycling and thermal stability, ball-milled Mg-
11 based amorphous alloy powders cannot be widely for the industrial wastewater
12 catalysis.

13 It is well known that the rate of chemical reaction is proportional to the rate of
14 electron transfer. Porous structures are widely used for catalysts due to its high
15 specific surface area. However, little work was done on preparing porous Fe-based
16 alloys as catalysts for dye degradation, mainly due to the electrochemical actively of
17 Fe. In this work, a porous Fe-based amorphous alloy was fabricated by dealloying
18 $\text{Fe}_{72}\text{Si}_2\text{B}_{20}\text{Nb}_6$ metallic glass. The selection of this metallic glass as an etching
19 precursor is based on the fact that Nb is both a glass forming element for Fe-based
20 alloys and an element which has a much lower standard electro potential than any
21 other elements in the Fe-Si-B system (Nd^{3+}/Nd : -2.323 V, Fe^{2+}/Fe : -0.44 V SiO_2/Si : -
22 0.92 V $\text{B}(\text{OH})_3/\text{B}$: -0.89 V). During the etching treatment, the Nd element is
23 preferential leached. Since the remaining Fe-Si-B is a good glass former and an ideal
24 system for dye degradation, a porous amorphous Fe-Si-B alloy with higher catalytic
25 activity can be obtained. To the best of our knowledge, this is the first time that a

1 porous amorphous Fe-based alloy has been prepared and it exhibits high catalytic
2 activity in the dye degradation.

3

4 **2. Experimental details**

5 The master alloy ingots, with a nominal composition of $\text{Fe}_{72}\text{Si}_2\text{B}_{20}\text{Nb}_6$, were
6 synthesized by arc melting a mixture of pure Fe, Si, B and Nb elements in a WK- II
7 vacuum arc melter under an Ti getter purified argon atmosphere. Subsequently, the
8 prepared ingots were remelted eight times to guarantee a uniform distribution of the
9 elements. Metallic glassy ribbons were then fabricated by injecting the melted master
10 alloy onto a spinning copper roller under an argon atmosphere. The glassy state of the
11 as-spun ribbons was confirmed by standard X-ray diffraction (XRD) analysis with
12 Cu-K_α radiation. Glassy ribbons with porous surfaces were prepared by an etching
13 technique: the as-spun ribbons were immersed in hydrofluoric acid (HF) solution for
14 free corrosion. The volume concentrations of the HF solution and etching duration
15 were used to further tailor the porous structure. After the etching treatment, all
16 samples were rinsed with distilled water and dehydrated alcohol before the catalytic
17 tests. A Jeol JSM-6490 scanning electron microscope was used to examine the surface
18 morphology of the specimens. The specific surface area of the as-spun and etched Fe-
19 Si-B-Nb ribbons was measured by the Brunauer-Emmett-Teller (BET) method using a
20 Belsorp-Mini-II analyzer.

21 Direct Blue 15 (DB 15) solid reagent was directly dissolved in deionized water to
22 form a simulated azo dye solution with a concentration of 100 mg/L. Hydrogen
23 peroxide with a dosage ranging from 2.9 mM to 58.2 mM was added into the azo dye

1 solution and the ribbon samples were then immersed in a DB 15-containing solution
2 for degradation testing. The dosage of the ribbons was kept at 0.03 g/L. About 4 mL
3 of the solution was taken out and filtered in a 0.45 μm membrane over a time interval
4 of 5-10 min during the degradation tests. The filtered samples were subjected to UV-
5 vis spectrum scanning where an excitation wavelength of 598 nm was used. The DB
6 15 solution degradation rate (R) was calculated by $R=(C_t/C_0) \times 100\%$, where C_0 is the
7 original DB 15 concentration and C_t is the DB 15 concentration at a given time,
8 respectively.

9 **3. Results and Discussion**

10 Fig. 1 shows the XRD patterns of the as-spun $\text{Fe}_{72}\text{Si}_2\text{B}_{20}\text{Nb}_6$ ribbons and the
11 samples treated with HF solutions. The as-spun ribbon exhibits only a broad
12 diffraction peak centered at a 2θ of about 45° , indicating the formation of an
13 amorphous structure in the original ribbon. The ribbons immersed in the HF solutions
14 for different durations show similar XRD patterns as the as-spun sample,
15 demonstrating that the etched ribbons are still amorphous after the HF treatment.

16 Fig. 2(a) and (b) show the surface morphologies of the $\text{Fe}_{72}\text{Si}_2\text{B}_{20}\text{Nb}_6$ ribbon which
17 are etched in the 20 % HF solution for 20 min and 40 min, respectively. After 20 min
18 of etching treatment, a uniform nanoporous structure with a pore size ranging from
19 100 nm to 200 nm forms on the surface of the ribbons. The longer etching time (eg.
20 40 min) leads to smaller pores, i.e. 50-100 nm. This phenomenon is related to the
21 different corrosion rates across the thickness direction of the ribbons. During the melt
22 spinning process, the ribbon surface which is contacted with the copper roller
23 undergoes the fastest cooling rate, whereas the other side of the ribbon experiences
24 the slowest one. The stress across the thickness direction of the ribbon changes from

1 compressive to tensile, resulting in a higher stress concentration on the surface of the
2 ribbons. As a consequence, the corrosion rate is higher on the surface of the ribbons.
3 At the beginning of the etching process, the first several atomic layers on the ribbon
4 surface are attacked by pitting corrosion where the Nb element is preferentially
5 leached, followed by the further sacrificial anodic corrosion of Si, B and Fe nearby.
6 Thus the pores grow and become connected until these layers are totally etched off.
7 Since the corrosion rate is higher on the ribbon surface, when the upper layers near
8 the ribbon surface are etched off gradually, more underlying smaller pores can be seen,
9 giving the appearance of the pore size decreasing with increasing etching time.

10 Fig. 3 shows a typical UV-vis spectra development as a function of the degradation
11 time (the ribbons etched in 20 % HF for 40 min are used as the catalyst). The original
12 DB 15 solution has a strong absorption peak at 599 nm and the intensity of the peak
13 becomes weaker during the degradation treatment. After 60 min, the solution is fully
14 transparent and no characteristic peak can be found in the UV absorption spectrum.
15 The DB 15 solutions treated by other Fe-based alloys have similar UV-vis spectra
16 development with degradation time. Based on the UV-vis results, the DB 15
17 degradation rate was calculated and summarized in Fig.4. As can be seen, all the
18 solutions follow the first order kinetic model: $C_t/C_0 = \exp(-kt)$, where k is the reaction
19 rate and t is the degradation time. When the solution is treated for 60 min, the one in
20 which no catalyst is added (control sample) exhibits the lowest degradation rate of
21 about 80%. In contrast, the solutions that contain as-spun or porous Fe-based ribbon
22 catalysts show a degradation rate of 80 % after only 10-30 min and a full
23 decomposition can be obtained after 30-60 min. The degradation speed of the
24 solutions with different catalysts is in the following order: as-spun $\text{Fe}_{72}\text{Si}_2\text{B}_{20}\text{Nb}_6$
25 amorphous ribbon < porous ribbon treated in 10% HF for 40min < porous ribbon

1 treated in 20% HF for 20min <porous ribbon treated in 20 % HF for 40min. It should
2 be noted that the porous ribbon treated in 20 % HF for 40min has significantly higher
3 catalytic activity than the as-spun ribbon, i.e. after 30 min of degradation, the DB 15
4 solution with the porous ribbon is almost fully decomposed while the one with the as-
5 spun ribbon decomposed after 60 min. To clarify the origin of the much higher
6 catalytic activity of the porous amorphous ribbon, the specific surface area of several
7 selected samples is measured. The results show that the ribbons etched in 20 % HF for
8 0 min, 20 min and 40 min have specific surface areas of about 0.025 m²/g, 0.092 m²/g
9 and 0.647 m²/g, respectively. When compared with the as-spun ribbons, it can be seen
10 that the etching treatment for 40 min leads to a dramatic increase in the specific
11 surface area by 25 times. The much higher specific surface area of the ribbon etched
12 for 40 min is shown to contribute to the notable improvement of the catalytic activity.

13 Since it shows the highest catalytic activity among all the samples in this work, the
14 ribbon which experienced 40 min of etching treatment in 20 % HF solution was
15 chosen for further experiments. Firstly, we studied the reaction kinetics of this porous
16 ribbon by measuring the degradation rate dependence on the reaction temperature.
17 Fig. 5(a) shows the degradation rate of DB 15 at various temperatures. Temperature
18 has a great effect on both the degradation rate and speed, demonstrating that the
19 reaction is a thermally activated process. The activation energy of the process can be
20 obtained according to the Arrhenius equation (Herney-Ramirez et al., 2008): $\ln k = -$
21 $E_a/RT + \ln A$, where k is the reaction rate constant, E_a is the activation energy, R is the
22 gas constant, and A is a constant. The Arrhenius plot is presented in Fig. 5(b) by
23 plotting $\ln k$ against $1/T$. The E_a for the degradation process is 34.6 kJ/mol, which is
24 much lower than that of a similar reaction (60-250 kJ/mol) using hydroxyl-Fe pillared
25 bentonite or as-spun Fe-based metallic glass as catalyst (Chen and Zhu 2007, Wang et

1 al., 2014).

2 Fig. 6 shows the effect of H₂O₂ dosage on the decolorization of DB 15 with the
3 porous amorphous ribbon. The reaction rate is sensitive to the H₂O₂ dosage. It first
4 increases greatly with the increasing H₂O₂ dosage (from 2.9 mM to 5.8 mM). Further
5 increase in H₂O₂ dosage (from 5.8 mM to 58.2 mM) leads to a decrease of the
6 reaction rate. The results suggest that Fenton-like degradation is the dominant reaction
7 where the reactions $\text{Fe}^0 + \text{H}_2\text{O}_2 \rightarrow \text{Fe}^{2+} + 2\text{OH}^-$ and $\text{Fe}^{2+} + \text{H}_2\text{O}_2 \rightarrow \text{Fe}^{3+} + \text{HO}\cdot + \text{OH}^-$
8 (Wang et al., 2014) take place. In this case, the amount of HO· which exhibits
9 stronger activity with azo dye plays a critical role on the degradation rate and speed.
10 When the H₂O₂ concentration is low, the solution cannot provide sufficient HO·,
11 leading to a lower reaction rate and speed. However, when the H₂O₂ concentration is
12 too high, the reaction $\cdot\text{OH} + \text{H}_2\text{O}_2 \rightarrow \text{H}_2\text{O} + \text{HO}_2\cdot$ (Liao et al., 2009) can take place
13 and reduces the effective ·OH amount. Thus the solution containing 5.8 mM of H₂O₂
14 shows the highest catalytic activity. Though the dominant reaction is a Fenton-like
15 one, it may not be able to exclude the possible effects of the reduction-type reactions
16 in this work. It has been reported that Fe-based metallic glass can react directly with
17 azo dye, i.e. the Fe atoms lose 2 or 3 electrons and form Fe²⁺ or Fe³⁺ ions, while the
18 N=N- bonds of the azo dye are broken by reduction, and form -NH₂ (Wang et al.,
19 2014). Further work is needed to fully understand this effect of the reduction-type
20 reaction in the system.

21 Fig. 7 shows the degradation rate of the solution with different DB 15
22 concentrations versus reaction time. It can be seen that in a wide DB 15 concentration
23 range (100-500 mg/L), the degradation rate can reach 90 %, suggesting that the
24 porous Fe-Si-B-Nb amorphous ribbon has great potential to be used in dye wastewater

1 degradation.

2 The stability and reusability of the porous ribbon have been evaluated by
3 degradation cycles and the results are shown in Fig. 8. There is a slight decrease in the
4 degradation speed. During the first use of the porous catalyst, the DB 15 solution
5 decomposes after 30 min. The second use of the catalyst delays the complete
6 degradation time by 10 min. Further reuse of the porous ribbons makes the complete
7 degradation time approach a stable duration of about 60 min. Though the degradation
8 speed decreases after second time of reuse, the degradation rate does not change
9 greatly, even after the 5th cycle of use. All the DB 15 solutions can be completely
10 decomposed within 60min and the degradation rate and speed is higher than the as-
11 spun ribbon sample, indicating that the porous metallic glass ribbon has good
12 reusability with no activity loss.

13 The ribbons subjected to the 1st and 2nd degradation tests were chosen for further
14 SEM observation. When compared with the as-etched porous ribbon (Fig. 9 (a)), the
15 sample used one time for degradation displays an irregular surface morphology (Fig. 9
16 (b)). Instead of fine pores, some loose oxidation products distributed on the surface
17 are observed. The EDS pattern (Fig. 9 (c)) shows that the main chemical compositions
18 of the sample are Fe, B, Si Nb and O. The high O content in the sample further
19 confirms that the irregular patterns and island-like areas are the oxidation products.
20 After the 2nd use in degradation tests (Fig. 9 (d)), the oxidation layer becomes much
21 thicker, and maintains a loose structure. The formation of the oxidation layer might be
22 the main reason that leads to the decrease in the degradation speed. Since the
23 oxidation products are of loose structure, the ribbon surface is still able to be exposed

1 to the DB 15 solution such that the degradation rate can still approach 100% for the
2 amorphous ribbons, even after several cycles of reuse.

3

4 **5. Conclusions**

5 In summary, as-spun Fe-based metallic glassy ribbons and etched porous ribbon
6 samples were used to degrade DB 15 azo dye. The degradation rate and speed for the
7 sample which was etched in 20% HF for 40min was higher than the as-spun glassy
8 ribbons, indicating that the porous glassy ribbon has much higher catalytic acidity
9 in the decomposition of azo dyes. The dramatic enhancement of the specific area of
10 the porous metallic glass by etching may contribute to the improvement of the
11 catalytic activity.

12 **Acknowledgments**

13 The work described in this paper was fully supported by the Research Grants Council
14 of the Hong Kong Special Administrative Region, China (Project No. PolyU 511313).

15

16

17 **References**

18

19 Mester, T., & Tien, M., 2000. Oxidation mechanism of ligninolytic enzymes involved
20 in the degradation of environmental pollutants. *International Biodeterioration &*
21 *Biodegradation*, 46(1), 51-59.

22

23 Peralta-Hernández, J. M., Meas-Vong, Y., Rodríguez, F. J., Chapman, T. W.,
24 Maldonado, M. I., Godínez, L. A., 2008. Comparison of hydrogen peroxide-based
25 processes for treating dye-containing wastewater: decolorization and destruction of
26 Orange II azo dye in dilute solution. *Dyes and Pigments*, 76(3), 656-662.

27

1 Wojnárovits, L., Takacs, E., 2008. Irradiation treatment of azo dye containing
2 wastewater: an overview. *Radiation physics and chemistry*, 77(3), 225-244.
3

4 Malik, P. K., 2004. Dye removal from wastewater using activated carbon developed
5 from sawdust: adsorption equilibrium and kinetics. *Journal of Hazardous Materials*,
6 113(1), 81-88.
7

8 Santhy, K., & Selvapathy, P., 2006. Removal of reactive dyes from wastewater by
9 adsorption on coir pith activated carbon. *Bioresource Technology*, 97(11), 1329-1336.
10 Saratale, R. G., Saratale, G. D., Chang, J. S., & Govindwar, S. P., 2011. Bacterial
11 decolorization and degradation of azo dyes: a review. *Journal of the Taiwan Institute
12 of Chemical Engineers*, 42(1), 138-157.
13

14 Baeta, B. E. L., Lima, D. R. S., Silva, S. D. Q., & Aquino, S. F. D., 2015. Evaluation
15 of soluble microbial products and aromatic amines accumulation during a combined
16 anaerobic/aerobic treatment of a model azo dye. *Chemical Engineering Journal* 259:
17 936-944.
18

19 Lin, Y. T., Weng, C. H., Chen, F. Y., 2008. Effective removal of AB24 dye by
20 nano/micro-size zero-valent iron. *Separation and Purification Technology*, 64(1), 26-
21 30.
22

23 Ma, L., Zhang, W. X., 2008. Enhanced biological treatment of industrial wastewater
24 with bimetallic zero-valent iron. *Environmental Science & Technology*, 42(15), 5384-
25 5389.
26

27 Li, P., Song, Y., Wang, S., Tao, Z., Yu, S., Liu, Y., 2015. Enhanced decolorization of
28 methyl orange using zero-valent copper nanoparticles under assistance of
29 hydrodynamic cavitation. *Ultrasonics sonochemistry*, 22, 132-138.
30

31 Chen, B., Wang, X., Wang, C., Jiang, W., Li, S., 2011. Degradation of azo dye direct
32 sky blue 5B by sonication combined with zero-valent iron. *Ultrasonics sonochemistry*
33 18(5): 1091-1096.
34

35 He, Y., Gao, J. F., Feng, F. Q., Liu, C., Peng, Y. Z., Wang, S. Y., 2012. The
36 comparative study on the rapid decolorization of azo, anthraquinone and
triphenylmethane dyes by zero-valent iron. *Chemical Engineering Journal*, 179, 8-18.

1 Fu, F., Dionysiou, D. D., Liu, H., 2014. The use of zero-valent iron for groundwater
2 remediation and wastewater treatment: a review. *Journal of Hazardous Materials*, 267,
3 194-205.
4
5 Segura, Y., Martínez, F., Melero, J. A., Fierro, J. L. G., 2015. Zero valent iron (ZVI)
6 mediated Fenton degradation of industrial wastewater: Treatment performance and
7 characterization of final composites. *Chemical Engineering Journal*, 269, 298-305.
8
9 Xiao, J., Gao, B., Yue, Q., Gao, Y., Li, Q., 2015. Removal of trihalomethanes from
10 reclaimed-water by original and modified nanoscale zero-valent iron:
11 Characterization, kinetics and mechanism. *Chemical Engineering Journal*, 262, 1226-
12 1236.
13
14 Greer, A. L., 1995. Metallic glasses. *Science*, 267(5206), 1947.
15
16 Wang, W. H., 2009. Bulk metallic glasses with functional physical properties.
17 *Advanced materials*, 21(45), 4524-4544.
18
19 Guo, Y., Bataev, I., Georgarakis, K., Jorge, A. M., Nogueira, R. P., Pons, M., Yavari,
20 A. R., 2015. Ni-and Cu-free Ti-based metallic glasses with potential biomedical
21 application. *Intermetallics*, 63, 86-96.
22
23 Phan, T. A., Hara, M., Oguchi, H., Kuwano, H., 2015. Current sensors using Fe–B–
24 Nd–Nb magnetic metallic glass micro-cantilevers. *Microelectronic Engineering*, 135,
25 28-31.
26
27 Schroers, J., 2008. On the formability of bulk metallic glass in its supercooled liquid
28 state. *Acta Materialia*, 56(3), 471-478.
29
30 Wang, J. Q., Liu, Y. H., Chen, M. W., Louzguine-Luzgin, D. V., Inoue, A.,
31 Perepezko, J. H. 2012. Excellent capability in degrading azo dyes by MgZn-based
32 metallic glass powders. *Scientific reports*, 2.
33
34 Zhang, C., Zhu, Z., Zhang, H., Hu, Z., 2012. On the decolorization property of Fe–
35 Mo–Si–B alloys with different structures. *Journal of Non-Crystalline Solids*, 358(1),
36 61-64.
37

1 Liu, P., Zhang, J. L., Zha, M. Q., Shek, C. H., 2014. Synthesis of an Fe rich
2 amorphous structure with a catalytic effect to rapidly decolorize Azo dye at room
3 temperature. *ACS applied materials & interfaces*, 6(8), 5500-5505.
4
5 Scaglione, F., Battezzati, L., 2015. Metastable microstructures containing zero valent
6 iron for fast degradation of azo dyes. *Journal of Materials Science*, 50(15), 5238-
7 5243.
8
9 Y. Tang, Y. Shao, N. Chen, X. Liu, S. Q. Chen, K. F. Yao, 2015. Insight into the high
10 reactivity of commercial Fe-Si-B amorphous zero-valent iron in degrading azo dye
11 solutions, *RSC Advances* 5, 34032.
12
13 Das, S., Bandi, V., Arora, H. S., Veligatla, M., Garrison, S., D'Souza, F., Mukherjee,
14 S., 2015. Synergistic catalytic effect of iron metallic glass particles in direct blue dye
15 degradation. *Journal of Materials Research*, 30(08), 1121-1127.
16
17 Herney-Ramirez, J., Lampinen, M., Vicente, M. A., Costa, C. A., Madeira, L. M.,
18 2008. Experimental design to optimize the oxidation of Orange II dye solution using a
19 clay-based Fenton-like catalyst. *Industrial & Engineering Chemistry Research*, 47(2),
20 284-294.
21
22 Zhang, C., Zhu, Z., Zhang, H., Hu, Z., 2012. Rapid decolorization of Acid Orange II
23 aqueous solution by amorphous zero-valent iron. *Journal of Environmental Sciences*,
24 24(6), 1021-1026.
25
26 Wang, J. Q., Liu, Y. H., Chen, M. W., Xie, G. Q., Louzguine-Luzgin, D. V., Inoue,
27 A., Perepezko, J. H., 2012. Rapid Degradation of Azo Dye by Fe - Based Metallic
28 Glass Powder. *Advanced Functional Materials*, 22(12), 2567-2570.
29
30 Chen, J., Zhu, L., 2007. Heterogeneous UV-Fenton catalytic degradation of dyestuff
31 in water with hydroxyl-Fe pillared bentonite. *Catalysis Today*, 126(3),463-470.
32
33 Wang, X., Pan, Y., Zhu, Z., Wu, J., 2014. Efficient degradation of rhodamine B using
34 Fe-based metallic glass catalyst by Fenton-like process. *Chemosphere*, 117, 638-643.
35
36 Liao, Q., Sun, J., Gao, L., 2009. Degradation of phenol by heterogeneous Fenton
37 reaction using multi-walled carbon nanotube supported Fe₂O₃ catalysts. *Colloids
38 and Surfaces A: Physicochemical and Engineering Aspects*, 345(1), 95-100.

1 **Figure captions**

2 **Figure 1** XRD patterns of as-spun Fe-based metallic glass ribbon and samples after
3 etching treatment.

4

5 **Figure 2** The surface morphology of the Fe-based amorphous ribbons after etching
6 treatment in 20% HF solution for 20 min (a) and 40min (b)

7

8 **Figure 3** Typical UV-vis absorption spectra of Direct Blue 15 solution treated by the
9 porous Fe-Si-B-Nb ribbon which was etched in 20%HF solution for 40min (DB 15 :
10 100 mg/L, H₂O₂: 5.8 mM, 333 K)

11

12 **Figure 4** The degradation rate as a function of the reaction time (DB 15 : 100 mg/L,
13 H₂O₂: 5.8 mM, 333 K)

14

15 **Figure 5** The effect of temperature on the degradation rate of Direct Blue 15 solutions
16 (a) and the corresponding fitting plot of lnk versus 1/T (b), a porous Fe-Si-B-Nb
17 ribbon which was etched in 20%HF solution for 40min was used as the catalyst, (DB
18 15 : 100 mg/L, H₂O₂: 5.8 mM)

19

20 **Figure 6** Effect of initial H₂O₂ concentration on the degradation rate of Direct Blue15,
21 a porous Fe-Si-B-Nb ribbon which was etched in 20%HF solution for 40min was used
22 as the catalyst (DB 15 : 100 mg/L, 333 K)

23

1 **Figure 7** Effects of initial DB15 concentrations on the degradation rate of Direct Blue
2 15 solutions, a porous Fe-Si-B-Nb ribbon which was etched in 20%HF solution for
3 40min was used as the catalyst (H_2O_2 : 5.8 mM, 333 K)

4

5 **Figure 8** Cycle degradation test on Direct Blue 15 solutions, a porous Fe-Si-B-Nb
6 ribbon which was etched in 20%HF solution for 40min was used as the catalyst (DB
7 15 : 100 mg/L, H_2O_2 : 5.8 mM, 333 K)

8

9 **Figure 9** Surface morphology of the porous Fe-Si-B-Nb ribbon which was etched in
10 20%HF solution for 40min in as-spun state (a), after 1th of degradation test(b) and
11 after 2nd of degradation test(d), the EDS result of the sample in b (c)

Fig. 1

[Click here to download high resolution image](#)

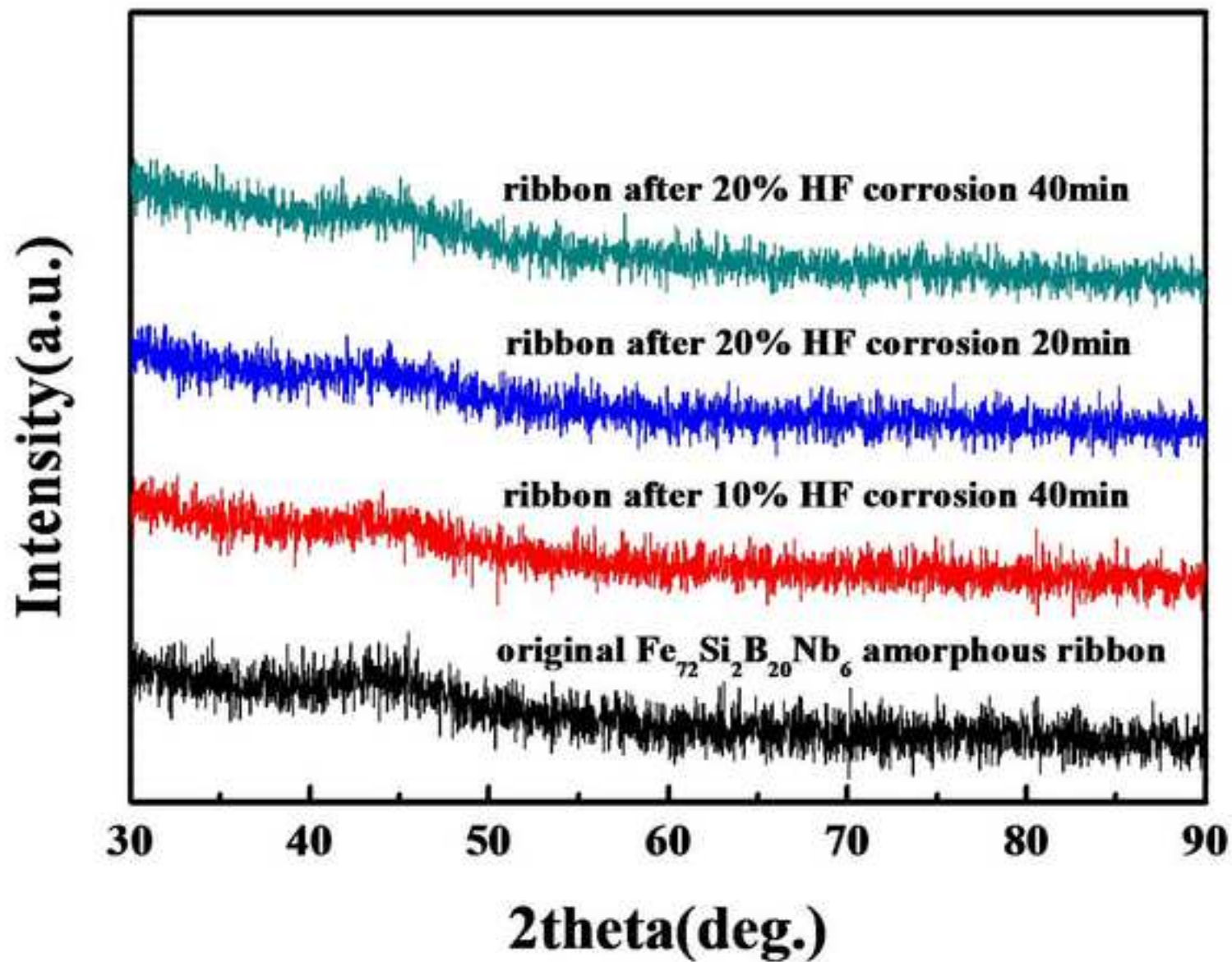


Fig. 2

[Click here to download high resolution image](#)

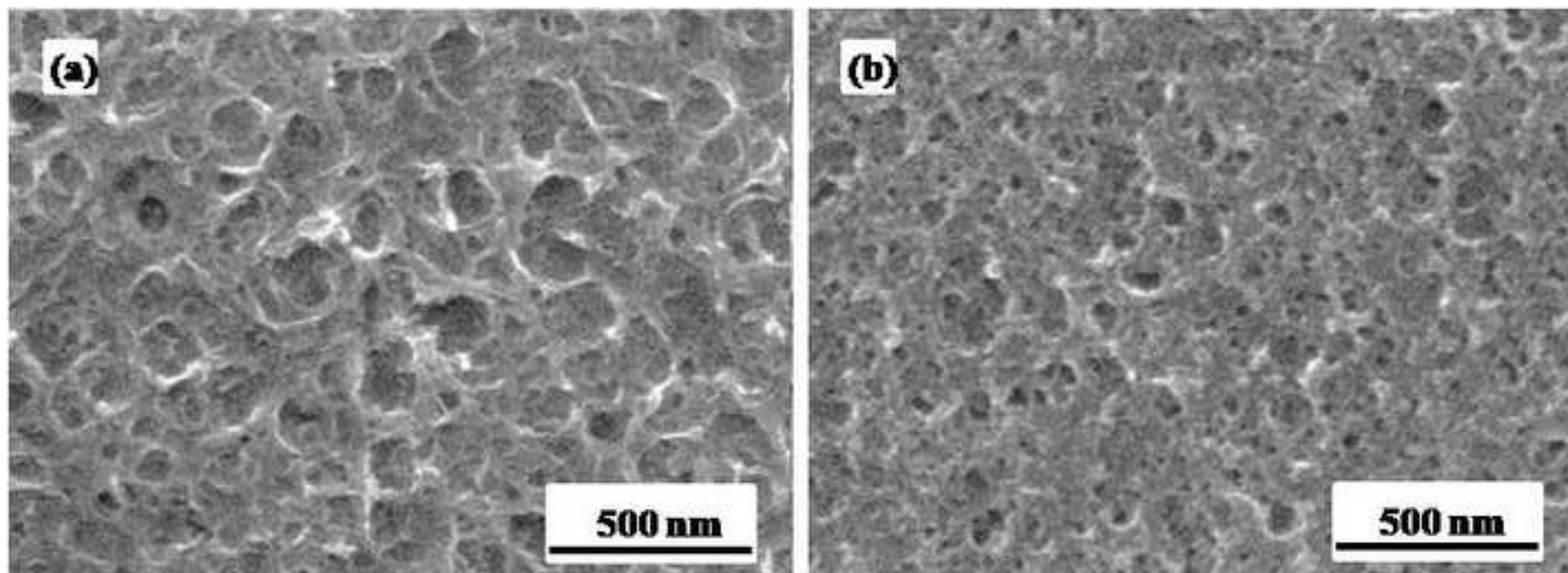


Fig. 3

[Click here to download high resolution image](#)

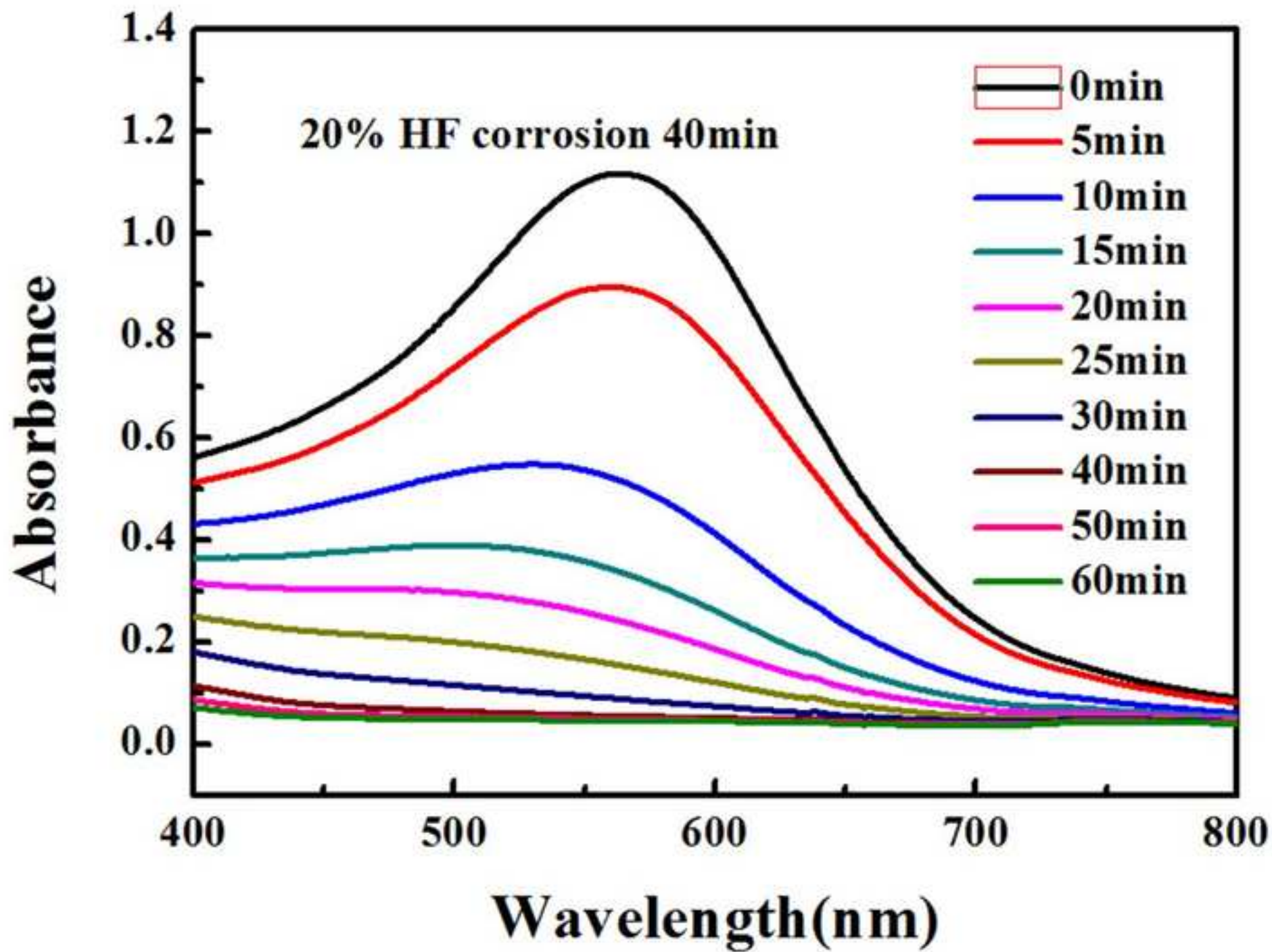


Fig. 4

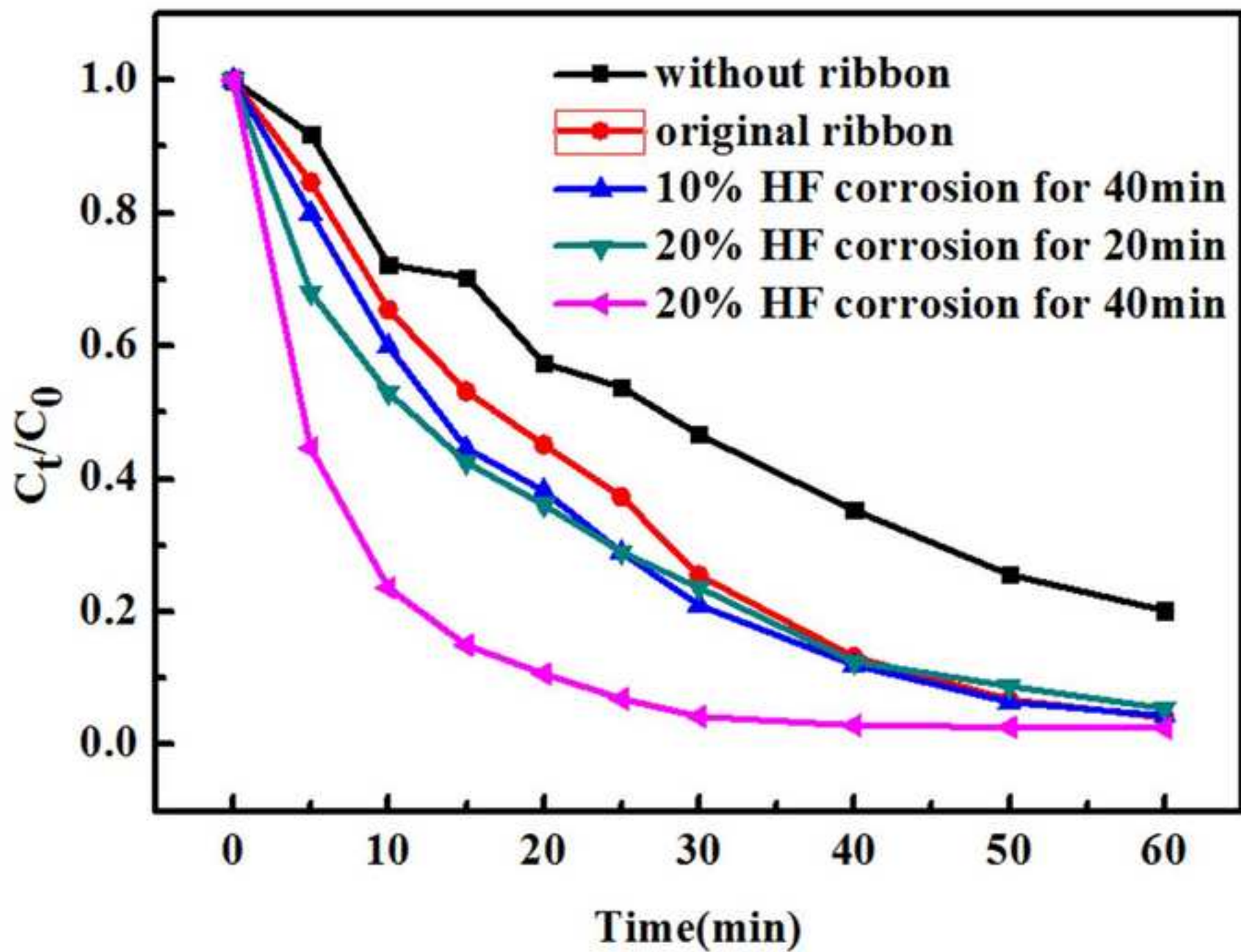
[Click here to download high resolution image](#)

Fig. 5a
[Click here to download high resolution image](#)

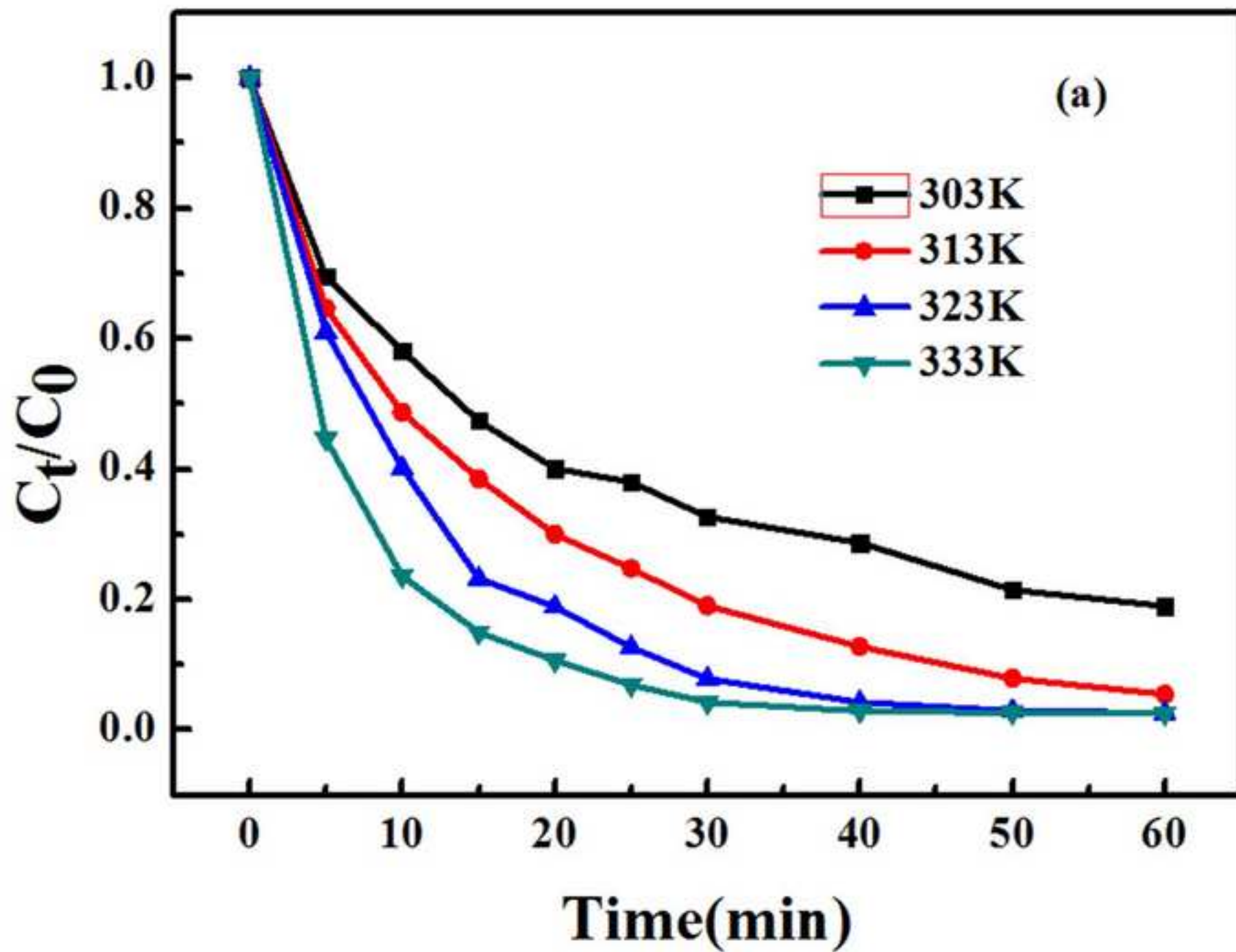


Fig. 5b

[Click here to download high resolution image](#)

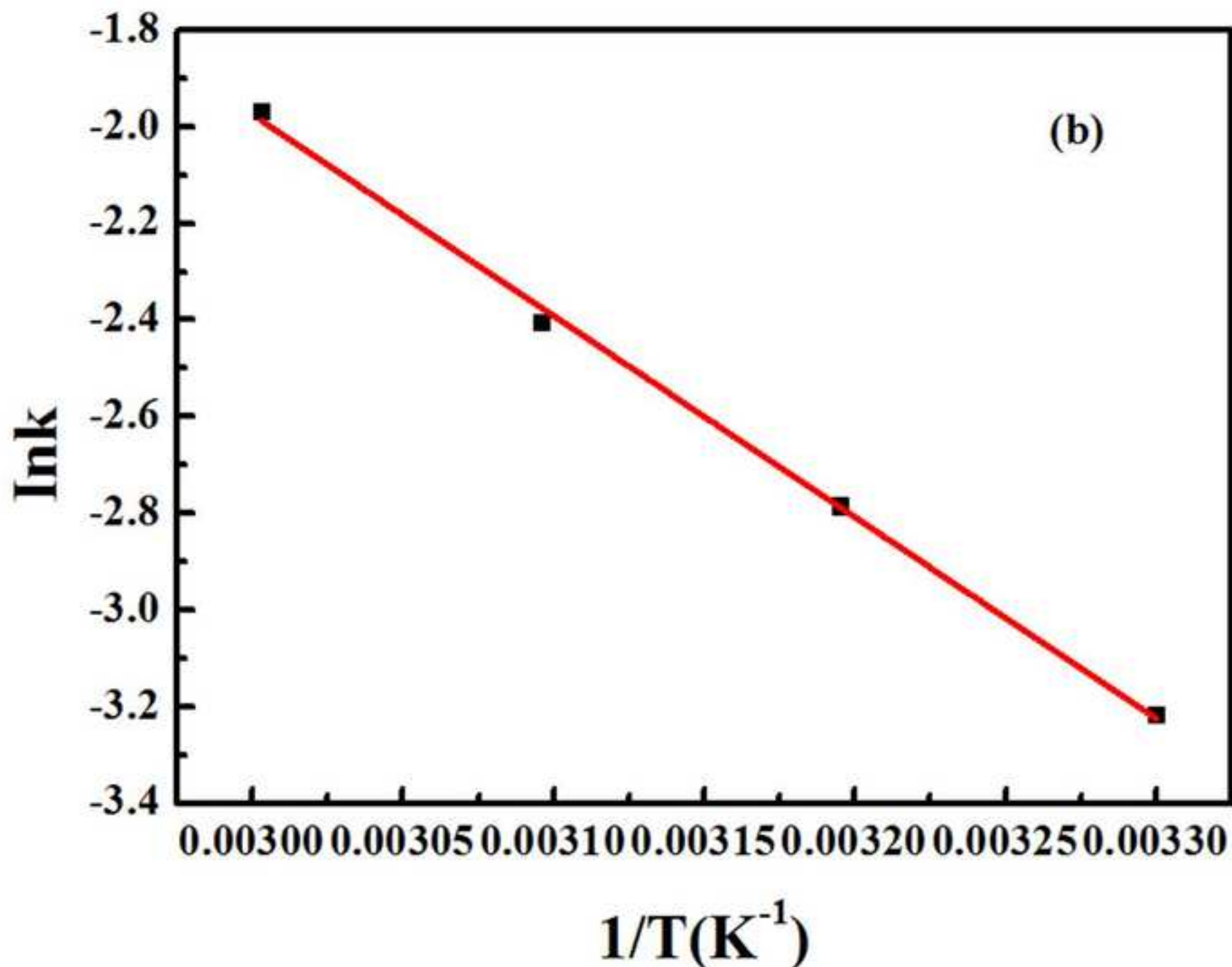


Fig. 6

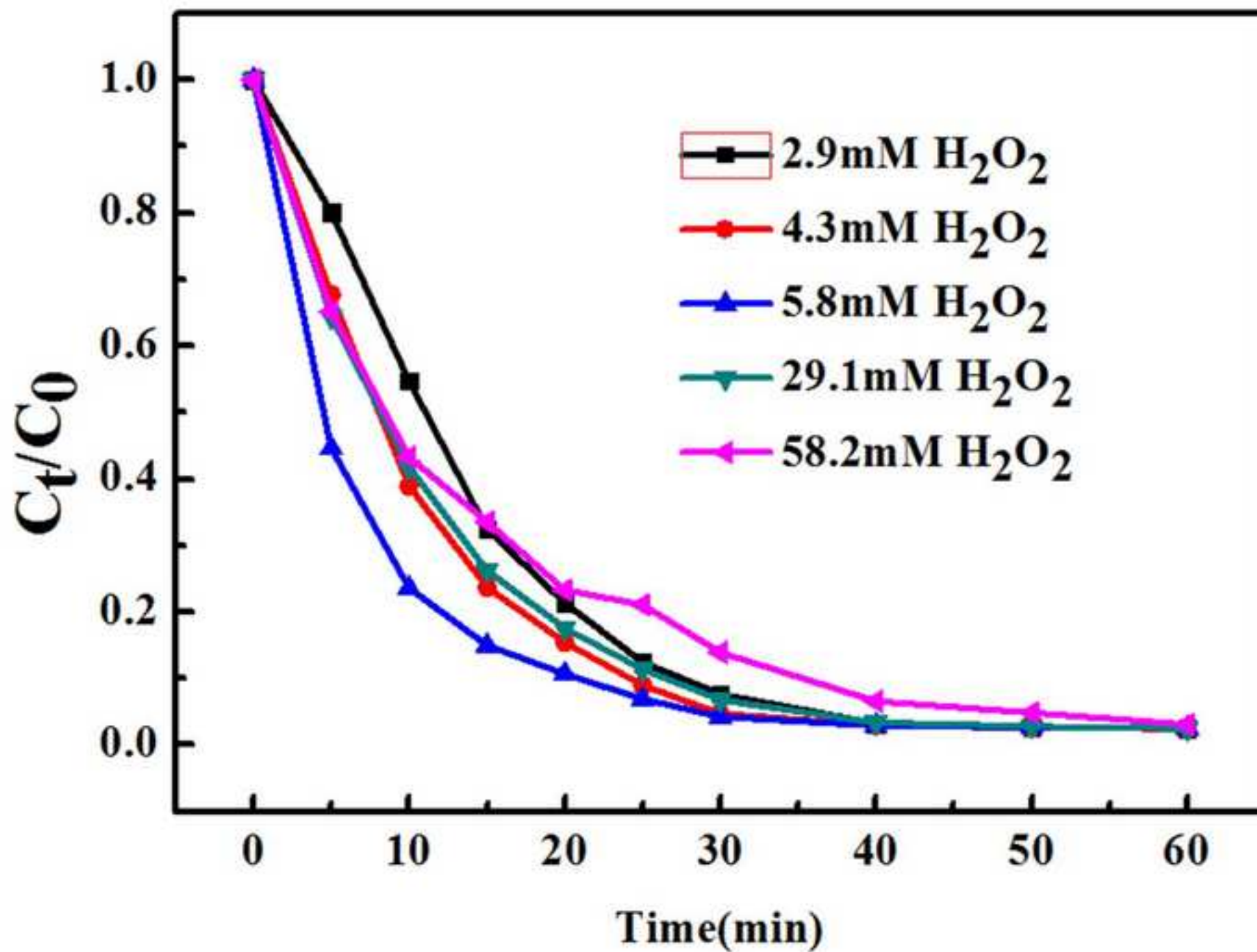
[Click here to download high resolution image](#)

Fig. 7

[Click here to download high resolution image](#)

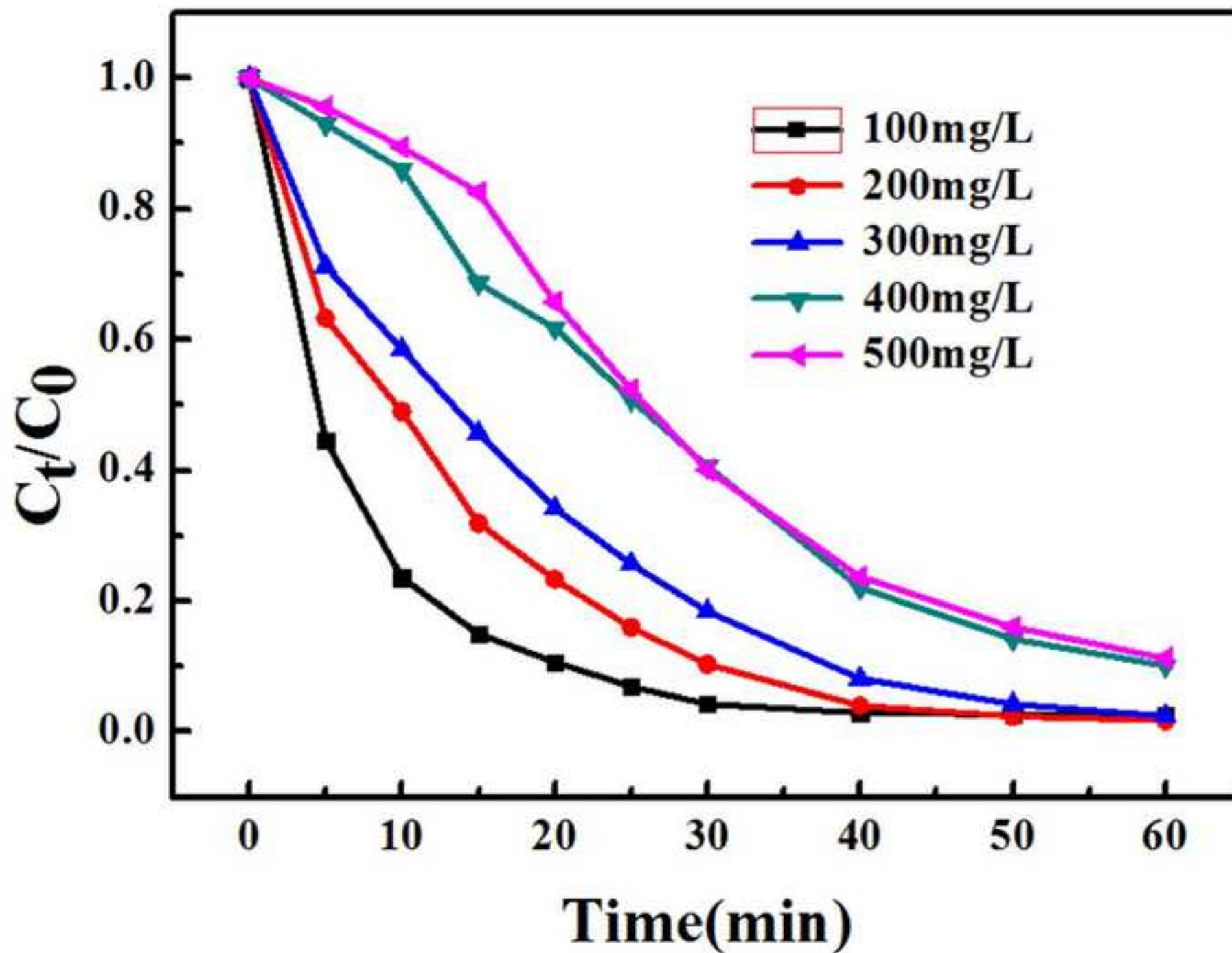


Fig. 8

[Click here to download high resolution image](#)

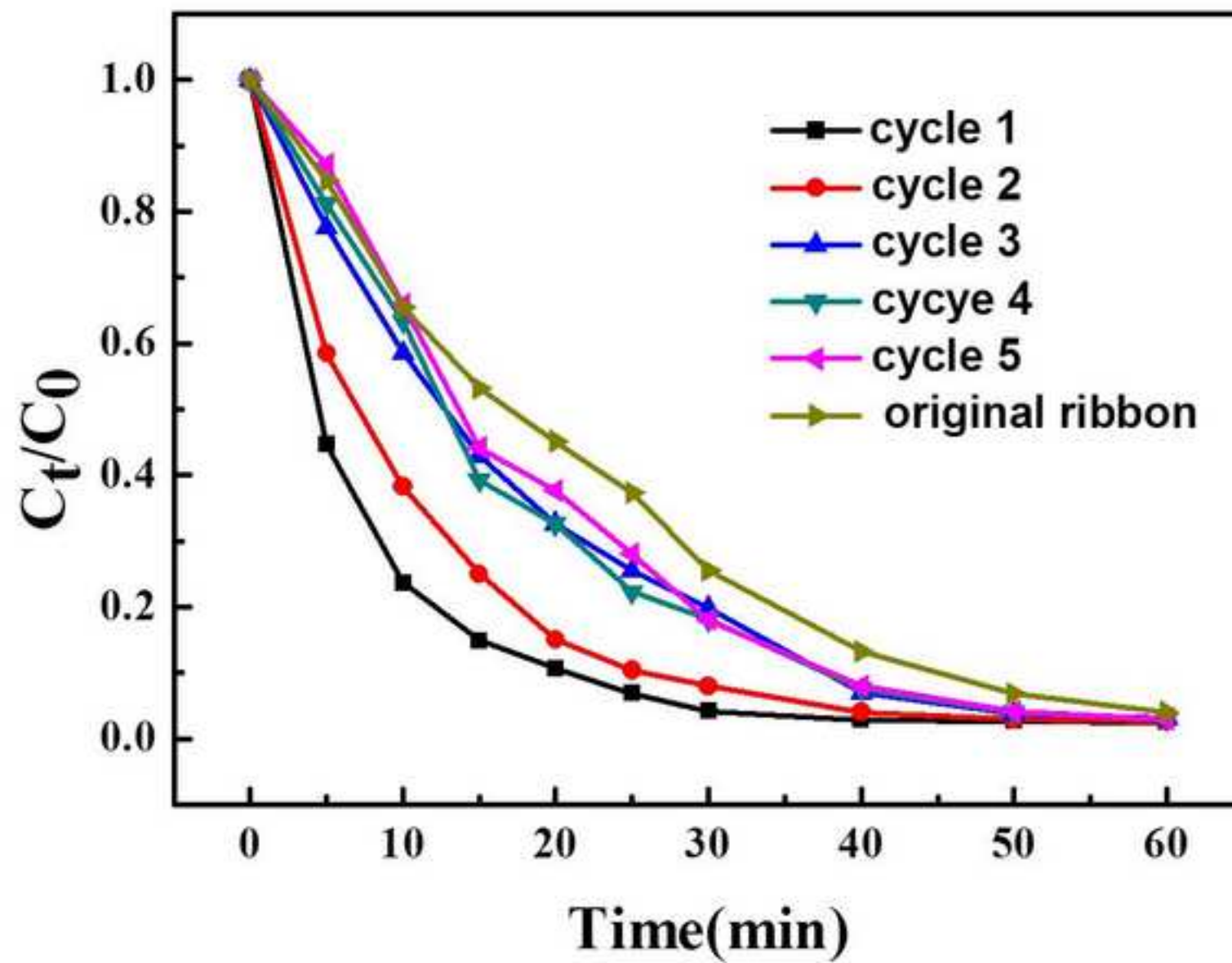


Fig. 9

[Click here to download high resolution image](#)

